



HAL
open science

CO₂-SCC in Flexible Pipe Carbon Steel Armour Wires

R. de Motte, G. Joshi, T. Chehuan, R. Legent, J. Kittel, N. Désamais

► **To cite this version:**

R. de Motte, G. Joshi, T. Chehuan, R. Legent, J. Kittel, et al.. CO₂-SCC in Flexible Pipe Carbon Steel Armour Wires. *Corrosion*, 2022, 78 (6), pp.547-562. 10.5006/4025 . hal-03748596

HAL Id: hal-03748596

<https://ifp.hal.science/hal-03748596>

Submitted on 12 Aug 2022

HAL is a multi-disciplinary open access archive for the deposit and dissemination of scientific research documents, whether they are published or not. The documents may come from teaching and research institutions in France or abroad, or from public or private research centers.

L'archive ouverte pluridisciplinaire **HAL**, est destinée au dépôt et à la diffusion de documents scientifiques de niveau recherche, publiés ou non, émanant des établissements d'enseignement et de recherche français ou étrangers, des laboratoires publics ou privés.

CO₂-SCC in Flexible Pipe Carbon Steel Armour Wires

R. De Motte,^{†,*} G. R. Joshi,^{**} T. Chehuan,^{***} R. Legent,^{*} J. Kittel,^{**} and N. Désamais,^{*}

^{*}Corresponding author. E-mail: rehananthony.demotte@technipfmc.com

^{*}TechnipFMC, Rue Jean Huré, 76580 Le Trait, France.

^{**}IFP énergies nouvelles, Rond-point de l'échangeur de Solaize BP3, 69360 Solaize, France.

^{***}TechnipFMC, Rio de Janeiro, Brazil.

ABSTRACT

Carbon Dioxide-induced Stress Corrosion Cracking (CO₂-SCC) is an environmentally assisted corrosion cracking phenomenon that has recently been identified as a new failure mode in flexible pipe armor wires. The phenomenon has been observed to take place notably in severe CO₂ environments and is a cause of great concern to the flexible pipe industry. Since its detection, a diverse and extensive testing program has been established to develop an understanding of the phenomenon and define safe application limits for carbon steel wires to prevent the initiation of CO₂-SCC. Several different testing methodologies have been explored and small-scale laboratory testing has played an instrumental role to this overall effort. This paper focuses on the results from three different small scale testing methodologies and the impact of different parameters such as CO₂ fugacity, temperature and confinement that play a crucial role in the initiation of CO₂-SCC. Furthermore, careful prominence has been given to the test set-up and methodology that has been rigorously developed over the last few years. With this developed protocol in place, CO₂-SCC has been effectively reproduced on all wire grades in a small-scale testing environment. Results have also shown that for a CO₂ fugacity greater than 15 bar and applied stress at 100% of the actual yield strength (AYS), all existing wire grades are susceptible to CO₂-SCC thus creating significant limitations to flexible pipe design with respect to this new failure phenomenon.

KEYWORDS: *Small scale testing, CO₂-SCC, flexible pipes, electrochemistry, applied stress, protective films.*

1 INTRODUCTION

Flexible pipes have been used by the oil and gas industry in offshore applications for many decades in the transportation of fluids. As shown in Figure 1, these complex pipelines are comprised of both polymer and steel layers; each layer independent but essential in its interaction with one another and fit-for-purpose¹. Carbon steel wires, present in the annulus region of the flexible pipe, are essential in providing the structure its high pressure and tensile load resistance. However, due to permeation, some of the components in the bore fluid can enter the annular space thus creating a corrosive environment for the carbon steel wires. Corrosive gases such as CO₂ and H₂S are present in the annulus dissolved in either condensed water, which permeates through the polymer pressure sheath, or seawater, as a result of damage to the external sheath. The extent of the corrosive nature of the annulus environment is dependent on the permeation rate and equilibrium pressure of acid gases².

Nevertheless, the corrosion rate of carbon steel wires present in the annulus of a flexible pipe is greatly reduced compared to what would be observed in water with similar partial pressures of acid gases via “conventional/non-confined” testing. This is due to the low confinement ratio (V/S) between the volume of electrolyte and the exposed surface of steel that is present in the annulus. The V/S ratio typically ranges from 0.01 to 0.1 mL/cm² that corresponds to a film of electrolyte of 10 to 100 μm at the steel surface thus resulting in a unique corrosive environment. The impact of this confinement has been studied in literature¹⁻⁵ and it has been identified that in such conditions, the environment is highly supersaturated in ferrous ions and the pH exceeds by far the natural bulk solution pH at saturation. In a study by Ropital et al.⁶, laboratory

1 testing showed that with the lowest confinement ratio that can be obtained for monitored experiments, at 20°C under 1 bar CO₂, the corrosion
2 rate was measured to be approximately 400 times lower than that in non-confined (high V/S) conditions. More explicitly, at the given conditions,
3 the CO₂ corrosion rate (determined by mass loss of coupons over 2-3 month-long exposures) was measured to be reduced from an average of 2000
4 µm/ year to approximately 5 µm/year when the V/S ratio is decreased from 100 to 0.25 mL/cm².
5
6

7 This particular behaviour observed in corrosion testing is a direct result of the high confinement present in a flexible pipe annulus which
8 is empirically known to inhibit corrosion by promoting both a local pH increase and protecting the steel surface with an insulating siderite (FeCO₃)
9 deposit⁷. FeCO₃, which is a by-product of the CO₂ corrosion process, precipitates on the steel surface thus creating a surface covering effect and a
10 diffusion barrier for corrosive species. The integrity of the FeCO₃ film depends on the characteristics of the film formed (coverage, porosity,
11 thickness, etc.) and plays a critical role in corrosion rate reduction in both confined and non-confined environments. In non-confined
12 environments, corroborating research⁸⁻¹⁰ has shown that “protective” corrosion product films generally form when the temperature is above 70°C
13 and pH above 6. Furthermore, the development of corrosion scale deposit over time and the protective states of film development have been
14 successfully characterized through the use of *in situ* electrochemical measurement techniques¹¹⁻¹⁵. In previous work¹², Electrochemical
15 Impedance Spectroscopy (EIS) measurements were carried out to compare the impedance response over time as a result of the film precipitation
16 kinetics in a non-confined environment at two different pH values (pH 6 and pH 6.6), pCO₂ of 0.54 bar and a temperature of 80°C. The study used a
17 combination of electrochemical and surface analysis techniques to study the impact of bulk solution pH on film formation kinetics and three
18 characteristic changes in the impedance behaviour were identified as a result of the developing film properties over time. In both conditions of pH
19 tested, the Nyquist curve initially features a single capacitive loop which is commonly attributed to a corroding metal surface. The capacitive loop
20 diameter (impedance) increases over time due to the precipitation of FeCO₃ which covers the surface and leads to a reduction in the active
21 corrodible surface area. After a longer duration of testing, the impedance spectra evolve for both conditions showing the appearance of a second,
22 smaller low-frequency capacitive loop which is interpreted to be an effect of the onset of mass transfer limitation (finite diffusion limitation)
23 through the scale as the scale further develops in its formation and further blocks/ protects the underlying steel surface. The high-mid frequency
24 (HMF) and low frequency (LF) semi-circle continue to increase in magnitude over time indicating a progressive development of the protective
25 corrosion product layer. This continues until the end of the test duration for the test at pH 6. However, for the test at a higher pH of 6.6, the
26 transformation of the LF time constant into a linear tail is observed after a period of 8 days. This is interpreted as the onset of diffusion-controlled
27 impedance (semi-infinite diffusion) and is believed to be the result of the evolution of the deposit layer towards a very high tortuosity. At this
28 stage, with the simultaneous transition to a more noble open circuit potential, it is considered that a “pseudo-passive” film has formed at this
29 higher pH thus indicating a superior state of protective film formation. Post-test analysis showed that the developed film was predominantly
30 FeCO₃. Magnetite (Fe₃O₄) was locally identified below the FeCO₃ film at both pH conditions thus showing no direct link to the observed “pseudo-
31 passive” behaviour at pH 6.6.
32
33
34
35
36
37
38
39
40
41
42
43
44
45
46
47
48

49 Despite the confined annulus environment of a flexible pipe being favourable to the formation of protective film formation and thus low
50 uniform corrosion rates, armour wires have been observed to be susceptible to crack formation in pure CO₂ operating conditions as shown in
51 Figure 2. This cracking phenomenon was first observed in flexible pipe armour wires in 2016 and identified to be CO₂-SCC. In 2017, a failure mode
52 alert was officially reported by the Brazil National Petroleum Agency (ANP) after the failure of a gas injection (GI) flexible pipe riser operating in a
53 severe CO₂ environment^{16,17}. CO₂-SCC is a form of environmentally assisted cracking and the result of the synergistic interaction between a
54 susceptible material, tensile stress and a specific corrosive CO₂-containing environment. The relevant literature for SCC occurring on carbon steels
55 in a CO₂ environment, predominantly in rigid oil and gas pipes, refers in general to two forms of SCC which are High pH SCC (HpHSCC) and Near
56
57
58
59
60

neutral pH SCC (NNSCC)¹⁸⁻²¹. HpHSCC has been observed to occur in concentrated bicarbonate or carbonate solutions associated with a pH of about 9 to 11 and has an intergranular morphology (cracks propagate along the grain boundaries between the grains). The crack formation is reported to be narrow, tight with almost no evidence of secondary corrosion of the crack wall. NNSCC, on the other hand, is characterized by a near-neutral pH (5.5 to 8) and primarily has a transgranular quasi-cleavage crack morphology (cracks propagate through the grains) with evidence of substantial corrosion of the crack wall. The crack morphology observed in flexible pipelines, as shown in Figure 2, is more similar to a NNSCC process presenting corroded walls and a transgranular crack morphology. Furthermore, the environments primarily responsible for NNSCC in rigid pipelines are generally confined environments, formed by the disbondment of the pipe coatings, as in the annulus of a flexible pipe. NNSCC has been previously associated with SCC in flexible pipe armour wires in a study by Campos et al²². However, despite the general alliance with this form of SCC, the understanding of the mechanism is still quite complex.

The NNSCC process mechanism is suggested to be a synergy between H₂ permeation and anodic dissolution¹⁸. From overall characterisation of cracks observed in field, CO₂-SCC has been observed to initiate from sites with localised pitting or “directly” from the metallic surface (i.e. without corrosion defects generating local stress intensity conditions). Possible factors influencing crack initiation in both cases may be inclusions, aligned surface defects, persistent slip bands produced by mechanical pre-treatment of the steel and/or pre-existing defects of the pipe material. It is believed that CO₂-SCC progression can be divided into an initiation phase and a propagation phase. An anodic mechanism seems to be more appropriate for explaining the CO₂-SCC initiation phenomenon which occurs in certain conditions resulting in localised corrosion which is due to local failure of the protective carbonate layer. Based on a general understanding of the influence of hydrogen in steels, it seems that hydrogen would not participate in CO₂-SCC initiation; however, there is a general agreement in the literature on the contribution of hydrogen in crack propagation. Hydrogen is, in particular, able to “segregate” in the plastic zone formed at the crack tip. However, a mechanism capable of significant hydrogen generation in a CO₂ environment that accounts for the protective iron carbonate film formation often found in the field with this form of cracking and compatible with the other mechanisms apparently active has not been clearly identified. In a paper by Colwell et al.²³, a mechanism for NNSCC is proposed capable of significant hydrogen generation for the near neutral scenario where hydrogen generation derives from the decomposition of bicarbonate as iron carbonate forms. In general CO₂-H₂O solutions, the first step in the mechanism is the evolution of carbonic acid (H₂CO₃), which forms through dissolution of CO₂. The article suggests that as the H₂CO₃ migrates to the active steel surface and corrosion occurs, FeCO₃ forms from the bicarbonate releasing H⁺ ions, which can then diffuse into the steel causing embrittlement or activating any other hydrogen related mechanism such as hydrogen-enhanced localized plasticity (HELP). The discussed role of hydrogen in secondary crack formation that start at specific sites i.e. inclusion or pits correlates with work carried out by Asher et al.²⁴ where the authors attribute it to the higher H dissolution rate at such defects. Furthermore, work carried out by Parkins et al.²⁵ showed that crack growth increased with increasing bicarbonate ion concentration suggesting that HCO₃⁻ is involved in the crack mechanism and further supporting the role of hydrogen in the cracking mechanism.

Since its discovery in flexible pipelines in 2016, CO₂-SCC has become a focal research point to flexible pipe manufacturers and a large variety of different test methods have been carried out to develop the understanding of this phenomenon. Within this work, a test methodology has been developed to effectively reproduce the initiation and propagation of SCC cracks in a representative environment of the field in the laboratory. This article focuses on presenting the results from three different small scale laboratory test methods that have been integral to understanding our material limits to CO₂-SCC. Combining results from separate electrochemical and applied load tests has improved the understanding of the impact of different parameters on the initiation/propagation of CO₂-SCC, including the kinetics of establishing pseudo-passive / diffusion-limited states. The formation of surface films is noted as an important factor affecting SCC and this article also aims to present the

1 characteristics of the protective films formed under different test parameters in order to identify the role that these phenomena play on a
2 material's susceptibility to CO₂-SCC.
3
4

5 **2 EXPERIMENTAL PROCEDURES**

6
7
8 The test campaign presented in this article considers two small scale applied load test methods with two different configurations: four-
9 point bending (4pB) and tensile load. Both test methods are widely used in the oil and gas industry to evaluate the resistance of metals to sulfide
10 stress cracking (SSC) and stress corrosion cracking (SCC) ^{26,27}. As shown in Figure 3 (a), 4pB test is a constant displacement test that is performed by
11 supporting a test specimen on two loading rollers and applying a load through two other loading rollers so that one face of the specimen is in
12 tension (uniformly stressed between the inner rollers) and the other is in compression. On the other hand, tensile load tests are constant load tests
13 used to evaluate a test specimen for environmentally assisted cracking (EAC) resistance under uniaxial tensile loading where dead weight, proof
14 ring or hydraulic loading may be applied. Figures 3 (a) and (b) show a photo of the interior of an open autoclave prior to testing for a 4pB test and
15 tensile test under hydraulic loading respectively. The third test method carried out within this study are electrochemistry tests. These tests were
16 carried out with electrochemical impedance spectroscopy (EIS) measurements in order to better understand the corrosion/ scaling responses of
17 the different material grades over time in different environments. As shall be discussed later in this article, the results from the electrochemistry
18 tests were used to provide a link between the film properties developed at the material surface and the susceptibility to CO₂-SCC identified through
19 applied load testing.
20
21
22
23
24
25
26
27

28 **2.1 *Materials and Preparation***

29
30 All steel wires used for testing are obtained directly from spool after having undergone the complete process at our suppliers,
31 straightened and cut to the required length. For the applied load tests, a series of carefully monitored steps are carried out to the test specimen
32 before application of the final load. The test sample is initially subjected to a 1% pre-straining deformation prior to being submitted to several four
33 point bending/ counter-bending cycles in order to achieve the maximum strain and cumulated plastic strain (PEEQ) representative of the
34 manufacturing process. This process is controlled using strain gauges and is based on inputs from finite element analysis (FEA) modelling.
35 Subsequently, a second 1% pre-straining deformation is applied in order to release any residual stresses in the test specimen and better control the
36 targeted level of stress during the final loading. This last step was determined through experience to be essential in order to effectively produce
37 reproducible test results and to minimize uncertainties caused by the stress pattern generated by the bending and counter bending protocol when
38 applying a final target stress level. Once these preparation steps are complete, the final stress level is applied as a targeted percentage of the
39 Actual Yield Strength (AYS) of the tested sample. In 4pB tests, strain gauges are used to control this final load step. It is to be noted that in all tests
40 (applied load and electrochemistry), prior to being introduced into the autoclave, all samples are thoroughly cleaned and degreased with acetone
41 in an ultrasonic bath and air dried. The samples are tested as-received and are not polished.
42
43
44
45
46
47
48
49

50 Almost all existing wire grades have been tested and studied as part of this work. However, in the following article, the results from three
51 tested armour wire materials (Steel A, B, C) are presented and discussed. The differences between the three steels are shown in Table 1 and Figure
52 4 shows their cross-sectional microstructure.
53
54
55
56
57
58
59
60

2.2 Overall Test Set-Up – Applied Load Tests

Figures 5 (a) and (b) show 2D schematics of the test set-up for 4pB and tensile load tests respectively. The test environment consists of an autoclave which is filled up to 80% of its volume with deaerated, CO₂-saturated synthetic seawater, prepared according to the ASTM D1141-98²⁸ standard, and with 20% of its volume serving as a gas headspace. During the test, CO₂ gas is introduced only in the gas headspace and not bubbled in the solution. This is carried out in order to prevent any perturbations to the test solution and to maintain a completely static environment. This is also more representative of what takes place in a flexible pipe annulus environment. As shown in Figure 5, the test samples are oriented vertically in the autoclave. In 4pB tests, the 4pB samples are tested with the samples half immersed and the waterline at the maximum stress level (between the two inner rollers). Additional steel coupons are exposed to the test solution to reach a confinement ratio (V/S) of 1.0 ± 0.2 mL/cm². For uniaxial tensile load tests, $\frac{1}{4}$ of the surface of the test sample is exposed to the gas headspace and steel coupons are also exposed to the water phase to ensure a proper confinement level. This unique configuration was determined to be essential and exposes the test samples to two types of confinement. The immersed region is exposed to a confinement ratio (V/S) of 1 ± 0.2 mL/cm². Within the non-immersed region of the sample, exposed to the gas headspace, a thin liquid water film is believed to form due to combined effects of capillarity and water condensation creating an extremely low confinement at this region of the sample. As shown in a study by Katayama et al.²⁹, the average thickness of water film that forms under similar conditions is expected to be approximately 10 – 100 μ m thus corresponding to a V/S ratio of less than 0.1 mL/cm² which is believed to be more representative of the confinement of a flexible pipe annulus. The minimum test duration for the applied load tests is 6 months. For tensile tests; however, the test can be shorter in case of rupture of the specimen. In order to validate a positive test result with no SCC, testing experience suggests a minimum duration of 6 months is required, whatever the loading procedure may be (4pB or tensile).

2.2.1 Post Test Analysis – Applied Load Tests

At the end of each test, before opening the autoclave, the solution pH and iron ion concentration is measured together with the CO₂ concentration through gas chromatography. These measurements are compared with existing tests and are used to validate that the test conditions were maintained as expected. The autoclave is then opened, and the test sample(s) is/are extracted and rinsed with distilled water. A macroscopic analysis is initially carried out prior to the corrosion scale being removed. The waterline and orientation of the sample is also identified clearly on the sample. Once the corrosion scale is removed using inhibited acid, according to ASTM G1-13, a Magnetic Particle Inspection (MPI) is carried out to locate cracks that may have been formed during the test. A metallographic cut is carried out for all identified indications to identify the crack profile (crack depth, branching, orientation, etc.) and are observed using an optical microscope. Furthermore, the test sample is also inspected for localized corrosion and metallographic cuts are equally carried out to identify the depth and width of the corrosion spot. This is carefully monitored as a high level of localized corrosion would result in an invalid test result with respect to SCC. In some tests, prior to the removal of the corrosion scale, the surface deposits along the sample are examined. Scanning electron microscopy (SEM) along with Energy-dispersive X-Ray analysis (EDX) is carried out to identify the differences in the film properties along the surface, the extent of the film coverage, and the differences in film morphology between the immersed and non-immersed areas of the sample during the test. Metallographic cuts were also carried out and analyzed to identify the thickness and characteristics of the protective film formed.

2.3 Electrochemical Tests

The following tests were carried out in environmental conditions similar to the stressed tests however with no applied stress component and with the test samples completely submerged. This was important, within this stage of the study, in order to effectively control the environment in which a specific parameter is tested and to have a clear understanding of the impact of this parameter on the development of the corrosion film. EIS measurements were carried out using a two electrode system³⁰ where one sample, the test sample, is used as the working electrode and a

1 second sample of the same material grade and identical dimensions is used as the reference/ counter electrode . A sinusoidal perturbation of ± 10
2 mV amplitude around their coupled potential difference was applied with a frequency range of 100 KHz to 5 mHz. Each test is carried out for a
3 duration of approximately two months or until the impedance measurements showed indication that the protective film formed is stable and has
4 attained an equilibrium steady-state in the tested environment. In addition to electrochemical measurements, supporting mass loss analysis was
5 carried out at the end of the test to determine the corrosion rate and essentially compare with the impedance results. Surface analysis was also
6 carried out in each test to study the deposit that formed on the surface i.e. the surface coverage, structure, and the thickness of the developed film
7 through SEM and EDX analysis.
8
9
10

11 **3 RESULTS & DISCUSSION**

12
13
14
15
16 The following chapter is divided into two sections. The first section focuses on qualitative surface observations of test samples,
17 characterizing the film formation and crack profiles observed throughout the surface of tested samples in stressed tests. The second section
18 discusses the results of three different parameters that have been investigated to identify their impact on the initiation of CO₂-SCC from both
19 electrochemistry and applied load testing. Applied load tests were carried out to identify whether the tested material grade is susceptible to CO₂-
20 SCC under specific conditions and help better understand/ define the boundaries for the occurrence of this cracking phenomenon.
21 Electrochemistry tests were employed to determine differences in the corrosion mechanism in these tested environments to identify what
22 contributes to the initiation of SCC cracks.
23
24
25
26
27

28 **3.1 Observed Crack Morphology and Differences in Protective Film Formation**

29
30 In all tests carried out within this work, cracks observed on the surface of tested samples (after scale removal) are systematically analyzed
31 to identify the crack profile. Figure 6 shows photos of cracks that were observed only on the non-immersed region of a tested sample under tensile
32 load as no cracks were observed on the immersed region. The test was carried out over a duration of 6 months, at 6 bar fCO₂, 40°C, with an applied
33 load of 100% of the AYS and on material grade Steel A. The specimens were etched (Nital) to reveal the microstructure and the relationship
34 between corrosion, microstructure and crack path. For the following test, very limited corrosion was observed across the tested sample with no
35 evidence of pits/ localized corrosion in the non-immersed region. The immersed region of the tested sample was observed to be relatively more
36 corroded with a few observations of localized corrosion/ pits. It is important to note that the relatively higher corrosion in the immersed region of
37 the samples is evident for all tests and can be attributed to the differences in confinement between the two regions of the sample. The cracks
38 shown in Figure 6 are representative of the different crack profiles observed across the non-immersed region of the sample. In general, they were
39 either found to be relatively thin and branched with the presence of secondary cracks as in the case of Figure 6 (a) or showed evidence of
40 preferential dissolution of ferrite along the crack path as shown in Figures 6 (b, c). All cracks were observed to initiate relatively from the surface of
41 the sample. Furthermore, as shown in Figures 6 (b) and (c), corrosion precipitates in the more profound cracks that formed during crack
42 propagation were not completely removed during inhibited acid descaling. Figure 7 shows the results of EDX analysis carried out on a magnified
43 image of the deposit identified within the crack path, with an atomic percent matching that of FeCO₃. The presence of this protective deposit may
44 prevent the continuous propagation of the crack resulting in it becoming dormant and preventing the failure of the tested specimen.
45
46
47
48
49
50
51
52
53
54

55 A wide variety of cracks with different morphologies have been observed during the different stressed tests carried out and a lot of
56 efforts have been made to associate characteristics of these cracks to the material grade and/or parameters being tested. This has been quite
57 complex and not always evident as in some cases, different morphologies may be present on the same specimen tested under the same condition.
58
59
60

1 However, clear differences have been observed between immersed and non-immersed region of the samples in each test. Cracks are found more
2 predominantly in the non-immersed region of the samples and, in most cases, no cracks were observed in the immersed region of the tested
3 sample as was the case for the test results shown in Figure 6. Furthermore, in most cases where cracks were observed in both regions of the
4 stressed sample, there was a higher likelihood that the cracks in the immersed region initiated from a pit and possessed wider profiles due to more
5 dissolution at the crack mouth and along the crack. This phenomenon is believed to be due to differences in the film properties that develops on
6 the surface as a result of a difference in confinement. Figure 8 shows an image of a stressed sample post-test prior to scale removal showing a clear
7 difference between the two regions of the sample. The figure shows results of a SEM analysis of the film formed on the surface of Steel C that was
8 exposed to 12 bar fCO_2 at 40°C, 100% of the AYS under tensile load over a duration of 6 months. On the immersed region of the sample, a clear
9 homogeneous film is observed. A combined SEM/EDX analysis showed the surface to be covered in $FeCO_3$ crystals with an average crystal size of
10 approximately 20-30 μm . A cross-sectional analysis showed a compact, almost dual layer of $FeCO_3$ film typical of that shown in Figure 9 (a).
11 However, in the non-immersed (gas phase) region of the sample, a cloudy-like surface appearance was observed and is shown in Figure 8. This is
12 representative of almost all tests carried out and upon further SEM/EDX analysis, it was shown that a heterogenous film was present across the
13 surface. In the darker region (2), $FeCO_3$ crystals were clearly observed to have formed on the surface but of a significantly smaller crystal size than
14 in the immersed region. The largest crystals observed on the surface were found to be approximately 11 μm and it is believed that below this
15 crystal formation in region (2) is a more nanocrystalline deposit layer as can be seen between some crystals and to the right-hand corner of the
16 image. This region has a lighter visual appearance; however, upon significant magnification (3), a clear crystalline morphology is observed. EDX
17 analysis across the surface suggested that the film formed in all instances was $FeCO_3$. However, the presence of chukanovite ($Fe_2(OH)_2CO_3$) or
18 magnetite (Fe_3O_4) traces may be present at the scale-substrate interface and is difficult to identify with a limited EDX analysis. Future X-Ray
19 diffraction (XRD) and/or Electron Backscatter Diffraction (EBSD) analysis is intended to further understand and characterize the developed film.
20 Figure 9(b) shows an SEM image of the cross-section of the film typically formed in the non-immersed region of the sample. The figure shows a
21 relatively thinner layer that spans across the entire surface.
22
23
24
25
26
27
28
29
30
31
32
33

34
35 In previous work ³¹, it was shown that under conditions more favorable to protective film formation, a higher surface saturation ratio
36 results in differences in the scale morphology due to the competition between the nucleation and growth processes. A more compact and dense
37 crystal formation is normally associated with a more protective film as larger crystals present on the surface implies a more dominant growth
38 process with fewer nucleation of crystals thus resulting a more porous layer. This difference in the film properties is apparent in the comparison
39 between the immersed and non-immersed regions of a tested sample. Whereas both regions are believed to be locally supersaturated in iron ions
40 with significantly high saturation ratio favorable to $FeCO_3$ nucleation and growth, it is hypothesized that the thin film that forms on the non-
41 immersed region at this high relative humidity environment creates a level of confinement ten times superior to that in the immersed region. It
42 may be justified that a superior nature of a protective film is present in the non-immersed region as in all tests, a higher level of corrosion (localized
43 or general) is observed in the immersed region. However, despite the apparently more protective nature of the film, this region is observed to be
44 significantly more susceptible to CO_2 -SCC. Figures 10 (a) and (b) show the non-immersed region of the sample analyzed in Figure 8 before and after
45 scale removal respectively. In this test, cracks were observed only in the gas phase region and the figure shows them to visually present across the
46 entire surface of this region with no observed link with the visual differences in the film formed. The properties of the film formed on a surface are
47 believed to play an important role in the susceptibility of a material to CO_2 -SCC and in the following section, three different parameters that have
48 been observed to have an impact on both CO_2 -SCC and film formation kinetics are investigated to further determine a link between these two
49 elements.
50
51
52
53
54
55
56
57
58
59
60

3.2 Parametric Study

3.2.1 Impact of Temperature

It is generally accepted that temperature plays a critical role in corrosion kinetics and in conditions favorable to that in which the solubility of iron carbonate is exceeded, increasing temperature accelerates the kinetics of precipitation and protective scale formation¹³. With this in mind, 4pB tests were carried out on Steel B at 10.1 bar $f\text{CO}_2$ with different levels of applied stress and temperature (25, 40, 80°C). The tested samples were completely immersed in the solution in order to more effectively control the parameter being tested. At the end of 6 months, CO_2 -SCC cracks were identified only at 40, 80°C and with an applied load of 100% of the AYS. Figure 11 shows images of cracks obtained at these two temperatures and clearly illustrates that a higher density of cracks was observed at 40°C. Based on these results, 40°C was identified as the optimum temperature for the initiation of CO_2 -SCC and utilised as the base temperature in testing the influence of other parameters. This particular observation was also reported in a study carried out by Santos et al.³² thus further consolidating the impact of this parameter.

Electrochemistry test results show characteristic differences in the corrosion behaviour and film formation kinetics over time at the three different temperatures tested 25, 40, 80°C and is shown in Figure 12. The tests were carried out in the same conditions as that in the applied load tests and on the same material grade Steel B (10.1 bar $f\text{CO}_2$, $V/S = 1$). In addition to EIS measurements, samples were also analysed post-test to determine the corrosion rate through mass loss and to understand the morphology of the corrosion deposits on the surface through surface imaging. Figure 13 shows the results of this analysis at 25°C, 40°C and 80°C. At all three conditions of temperature, the steel surface was visually observed to have a significant film coverage. This observation is a direct result of the high confinement present especially for 25°C where very limited film formation would be expected in a conventional non-confined environment. Despite the extent of film coverage observed visually for all three conditions, the properties of the film are quite different and this is made clear with the mass loss corrosion rate results. A significantly higher mass loss took place at 25°C and 40°C in comparison to that at 80°C with the highest mass loss corrosion rate recorded for a temperature of 40°C thus indicating important differences in the corrosion kinetics and the protective nature of the developed films. The higher mass loss at 40°C in comparison to that at 25°C is due to a significantly higher corrosion rate of the steel surface prior to development of the protective film. This is not clear from the impedance results shown in Figure 12 as the Nyquist plots show the characteristic changes in the impedance behaviour for each week thus masking the interfacial response during the first few days of testing. Figure 14 shows the instantaneous corrosion rate determined from the equivalent circuit fitting of the impedance spectra using the equivalent circuit and approach defined in¹² using a Stern-Geary coefficient of 52 mV/decade. The figure includes the results from the impedance measurements during the initial days of testing. It shows a significantly higher corrosion rate during the first few days of testing at 40°C which is responsible for the higher overall corrosion rate determined by mass loss measurements that are averaged over the entire test duration. The figure also shows that the initial corrosion rate is highest at 80°C due to faster corrosion kinetics prior to a rapid development of protective corrosion product scale on the steel surface. Mass loss and surface analysis are significantly useful elements; however, they remain quite limited in their approach with regards to understanding time-dependant evolution and in-situ events. Furthermore, in such conditions favourable to protective film formation due to Fe^{2+} ion supersaturation, subtle differences in the film porosity and the overall protectiveness in the film layer are more difficult to identify. In order to better understand the differences in the film, EIS results are utilised to track the corrosion related phenomena that takes place at the steel surface over time.

As discussed in the introduction, characteristic changes take place in the impedance behaviour as the result of the development of a protective film and these changes can be observed in the Nyquist plot representations at different exposure times. In Figure 12, impedance data have been plotted on the same scale at the three different temperatures tested allowing for a direct comparison between them. Figure 12 (a) and

(b) show that at 25°C, the Nyquist plot remains in the form of a capacitive semicircle over the total test duration of 8 weeks. The start of a second time constant is only detected at the 8th week. Over the first two weeks, the diameter of the single time constant decreases while maintaining the same profile suggesting an increase in the corrosion rate. This continues but at a slower rate until the 5th week of exposure after which the impedance starts to increase once again indicating a decrease in the corrosion rate. Coupled with the surface analyses, these EIS spectra suggest that Steel B corrodes for a long period at 25°C before starting to experience a relative protective state. It results in the formation of a thick corrosion scale (60 – 70 µm) with no diffusion barrier protection. In comparison, at 40 and 80 °C, EIS results show large impedances and linear tail like features at low frequency after only two weeks of testing at both conditions of temperature. This implies that a protective film of low porosity has precipitated on the steel surface and that the diffusion of corrosive species to the scale/ substrate interface has become constrained. Furthermore, after a period of 6 - 7 weeks, very few changes in the impedance curves are observed indicating that the film formed is quite stable and that an equilibrium steady-state has been reached. Comparing the results between 40 and 80°C, it is observed that at 80°C, the distinction between the first and second semi-circle (time constants) and the overall impedance is comparatively lower. This is expected to be an effect of a higher temperature which makes reaction kinetics higher / impedances lower and may not be assigned exclusively to higher or lower levels of corrosion protection. It can be deduced from the combined analysis of the applied load and electrochemistry test results presented above that CO₂-SCC takes place in conditions where a pseudo-passive film is likely to form as is observed at 40 and 80°C. In a confined environment, it is observed that film formation kinetics is relatively rapid and a stable protective pseudo-passive film is formed with a test duration of a few weeks at temperatures above 40 °C. The formation of this protective film is believed to be a pre-cursor to the initiation of SCC and its formation within a period of a few weeks supports the hypothesis that 6 months is a sufficiently long test period to reproduce CO₂-SCC in a small scale test environment. Furthermore, with these results, the importance of the surface state and protective film formation kinetics is further brought to light. It may be argued that a higher solution temperature favours the thermodynamics and kinetics of iron carbonate scale precipitation³³ which may end up protecting vulnerable localised corrosion or accessible microstructural heterogeneities at rates faster than the kinetics of crack nucleation under a static load. Through rapidly masking off vulnerable zones at the steel/scale/solution interface, the higher temperature could play an influential role towards limiting CO₂-SCC under these test conditions. One hypothesis is that vulnerable sites may remain accessible for longer in the 40°C +/- 15°C range, permitting localised corrosion, crack nucleation and propagation to proceed at faster rates than the retardation kinetics of scaling.

3.2.2 Impact of Confinement

As discussed previously, the exposed level of confinement has a strong impact on film properties and thus on the CO₂-SCC susceptibility of a given material tested. All applied load tests were carried out with test samples only partially immersed in the test solution thus creating two types of confinement at the surface of the samples. This configuration was adapted during the course of the test program as a result of post-test observations and is considered vital as the confinement created in the headspace/non-immersed region (estimated V/S ratio of less than 0.1) allows for a more relevant testing to what is observed in the annulus environment of a flexible pipe. Attaining this level of confinement in an immersed environment with a stress component and at high pressure is extremely difficult in a laboratory environment. Considering that no tests to-date have shown only cracks in the immersed region of a tested sample further highlights the need to understand this thin water film environment present in the non-immersed region to better understand CO₂-SCC in flexible pipe armour wires.

The impact of this parameter is further shown through the results of two tensile load tests in Figures 15 and 16. Figure 15 shows results from a test carried out on material grade Steel B with an applied stress of 95% of the AYS and at 40°C, 6 bar fCO₂. The test ended after 4.5 months due to the rupture of the test sample at the water line. In the following test, cracks have been observed in both regions of the sample. The cracks in

1 the immersed region of the sample were observed to have a maximum depth of 200 μm and comparatively thicker than that observed in the non-
2 immersed region. Furthermore, cracks were observed to initiate from pits due to higher levels of under-deposit, localised corrosion. In the non-
3 immersed region, the cracks were thinner and more branched with depths of approximately 630 μm closer to the rupture face. Figure 16, on the
4 other hand, shows an example of a test where cracks were only observed on the non-immersed region of the test sample. This particular tensile
5 load test was carried out on material grade Steel C with an applied load stress of 100% of the AYS and at 40°C, 15 bar $f\text{CO}_2$. As shown in the figure,
6 a large density of CO_2 -SCC cracks was observed in the non-immersed region which were found to be quite thin and deep with minimal branching. In
7 the immersed region, no cracks were observed. In the following test, a relatively low-level of corrosion was observed throughout the entire test
8 surface. It may be further added that the crack morphology on the tempered martensite steel grade C is usually observed to be straight and thin
9 with minimal branching and limited corrosion of the crack walls. This difference may be noted in comparison with cracks observed in Steel A and
10 Steel B shown in Figures 6 and 15 respectively where the crack path shows strong interactions with dissolution. This is believed to be the result of a
11 more homogenous microstructure and lower carbon content of the material suggesting that the crack path is more microstructure driven.
12
13
14
15
16
17
18

19 In order to help understand the impact of confinement on corrosion and protective film characteristics, electrochemistry tests were
20 carried out with a V/S ratio equal to 1 and 0.3 respectively. It is to be noted that although a gas phase exposure and an immersed exposure at low
21 V/S ratio are not exactly the same, the importance of this comparison lies in the relative understanding of film formation kinetics and the
22 observations of scale/ sub scale properties due to the higher confinement present in the latter. The tests were carried on Steel C at 40°C and 10.1
23 bar $f\text{CO}_2$. Upon comparing the Nyquist plots under the two conditions in Figure 17, it is clear that confinement has a significant impact on film
24 development over time with clear differences in the impedance behaviour. In Figure 17 (a-b), at a V/S ratio equal to 1, the Nyquist plot shows a
25 clear transition between the three characteristic phases in the impedance behaviour and a low frequency linear tail appears after a period of 6
26 weeks. In contrast, at a higher confinement (lower V/S confinement ratio) as shown in Figure 17 (c-d), EIS results shows that a protective film forms
27 at a significantly faster rate and a linear tail is observed only after a period of 2-3 weeks which signifies the early onset of diffusion impedance.
28 Furthermore, looking at the comparison between Figures 17 (b) and (d) which have been plotted in the same scale, it shows that a lower global
29 impedance is measured for a higher confinement. A classical interpretation of these spectra may indicate a lower protective character of the
30 corrosion product film at V/S = 0.3, suggesting a higher tendency for dissolution/ rupture. This could help explain the higher density of cracks
31 observed in the gas-phase region in the applied load tests. However, this hypothesis contradicts the results observed in Figure 12 showing the
32 impact of temperature. Comparing Figure 12 (d) and (f), EIS results show a lower total impedance at 80°C than that at 40°C where a higher
33 tendency to the initiation of CO_2 -SCC is expected and observed. Thus, further testing and a more in-depth analysis of impedance results is still
34 required to improve the understanding of these results. With this in mind, it is important to note nevertheless that clear differences in the
35 impedance behaviour is observed suggesting significant differences in the film properties at these different conditions. Furthermore, despite the
36 lower overall total impedance observed at 80°C, the impedance curves shown in Figure 12 (d) and 17 (d) are similar and qualitatively coincide with
37 conditions that are more favourable to the initiation of CO_2 -SCC.
38
39
40
41
42
43
44
45
46
47
48
49

50 **3.3 Impact of $f\text{CO}_2$**

51 So far, in the sections discussing the effect of temperature and confinement, results have shown that CO_2 -SCC cracks have been
52 reproduced in tests where a pseudo-passive film (presence of a linear tail) has been shown to have formed on the tested material surface. This
53 correlation helps to justify that the specific conditions created at the interface (local chemistry changes, local rupture) due to the presence of the
54 pseudo-passive film in applied load tests is likely a necessary precursor to initiate and propagate CO_2 -SCC. In conditions such as 10 bar $f\text{CO}_2$ at 25°C
55
56
57
58
59
60

(Figure 12 (a) and (b)), it is apparent that if the underlying steel surface continues to corrode in the presence of a semi-protective film, the interfacial conditions do not end up being harsh or localised enough to permit crack initiation.

The final parameter presented and discussed in this article is the impact of $f\text{CO}_2$. CO_2 fugacity has been observed to be critical to SCC testing, and along with applied stress, is considered to be the defining parameters for the development of CO_2 -SCC free domains. Over the last few years, through a large volume of applied load tests carried out, CO_2 -SCC cracks have been successfully reproduced on all material grades used by TechnipFMC in standard flexible pipe design with tensile or 4pB testing configuration. Results have shown that the SCC risk increases with an increase in $f\text{CO}_2$ with some materials being more resistant than others. Furthermore, at 100% of the AYS, all material grades were observed to be susceptible to CO_2 -SCC for a CO_2 fugacity greater than or equal to 15 bar. This shows a significant contradiction with the work done by Santos et al.³² where 4pB test results showed no CO_2 -SCC on a material grade tested at 80 bar $f\text{CO}_2$ and with an applied load at 100% of the AYS. It is believed that the reason behind this difference from our results may be linked to differences in the experimental set-up and sample preparation. Furthermore, the article³² shows no indications of SCC on a high strength sweet service wire tested at conditions of 10 bar and 40°C after a period of 180 days. In our work, CO_2 -SCC cracks were observed in sweet service, high strength wires (Steel A) in tests carried out with as low as 3 bar $f\text{CO}_2$ as shown in Figure 18 (a). The figure shows two selected cross-sectional microscope images that are believed to be representative of the overall cracks observed along the surface at 3 bar and 6 bar respectively. It is to be noted that cracks were observed only in the non-immersed region of the sample. Both tests were tensile load tests carried out on Steel A, at 40°C, 100% of the AYS and over a duration of 6 months. Figure 18 shows an interesting impact of $f\text{CO}_2$ on the crack morphology for the tested steel grade. It was observed that for the same material grade, increasing the $f\text{CO}_2$ resulted in finer, more branched cracks with relatively lower preferential dissolution along the crack path. Figure 6 shows additional images for the same test shown in Figure 18 (b).

Figure 19 shows the impedance curves for Steel C tested over a duration of 8 weeks at 40°C, $V/S = 1 \text{ mL/cm}^2$ at 1 bar $f\text{CO}_2$, 15 bar $f\text{CO}_2$, and 22 bar $f\text{CO}_2$. The results show that a single capacitive semi-circle is observed for the entire test duration for the test at 1 bar $f\text{CO}_2$, with no linear tail evident at low frequency. Figures 19 (b) and (c) depict impedance curves for Steel C at 15 and 22 bar $f\text{CO}_2$ respectively. These test results show that an increase in $f\text{CO}_2$ results in a more rapid formation of a pseudo-passive protective overlayer. For a test duration of 8 weeks, it has been shown that a protective pseudo-passive film does not form at 1 bar (Figure 19(a)) and forms after 6 weeks, 3 weeks, 2 weeks for 10 bar (Figure 17), 15 bar and 22 bar (Figure 19 (b) and (c)) respectively confirming a faster film formation kinetics with an increasing $f\text{CO}_2$. The rapidity of the transition to a pseudo-passive state appears to be an important parameter towards the severity in CO_2 -SCC crack observations. Furthermore, in conditions where a linear tail is formed, the modulus of the total impedance at 1 mHz is observed to be approximately $1000 \times 10^3 \Omega \cdot \text{cm}^2$, $120 \times 10^3 \Omega \cdot \text{cm}^2$ and $55 \times 10^3 \Omega \cdot \text{cm}^2$ thus showing a decrease with an increase in $f\text{CO}_2$. This again goes to suggest that despite the more rapid formation of a pseudo-passive protective film, it may be of poorer characteristics (i.e. more permeable) thus increasing the susceptibility to CO_2 -SCC. A rather important aspect observed in Figure 19 is that the impedance curves after a period of 6 weeks start to overlap/ superimpose. This is interpreted as the establishment of an interface that is stable and at a steady state with the surrounding solution chemistry. Such EIS observations suggest that the interface will not continue to develop to a great extent over a longer duration of testing.

The results presented in the present article address the main developments in our understanding of CO_2 -SCC in a flexible pipe environment; however, uncertainties still exist related to this failure mechanism. In future work, a large amount of similar testing and further characterization of the precipitated film is planned in order to further enhance the understanding of the above tested parameters and other essential parameters such as H_2S . Furthermore, reservations still exist on the mechanism behind CO_2 -SCC. A more targeted test framework is

intended to help clarify whether the process is a pure anodic process or rather a mixed anodic and hydrogen mechanism. CO₂-SCC free domains have been built for the existing material grades and certified by Bureau Veritas; however, efforts are underway to extend these domains for lower stresses. Lastly, electrochemistry tests have proved fundamental in developing our understanding and has added value through its correlation with applied load tests. However, one main limitation is that electrochemistry tests and applied load tests have been carried out separately. EIS tests on loaded specimens would prove invaluable moving forward and are planned within the future work.

4 CONCLUSIONS

CO₂-SCC in flexible pipes is a relatively new and complex failure mode that has strongly impacted the entire flexible pipe industry since 2016. Upon its discovery, a large amount of resources have been attributed to understanding this phenomenon to improve flexible pipe design and define a safe, certified domain in which there is no risk of CO₂-SCC. The relevant work carried out is extremely diverse and includes improving the understanding and prediction of the conditions within the annulus and executing small scale and full scale testing to help develop SCC free domains for existing material grades. The results presented in this article focuses on presenting the results of small scale tests that represent a vital part of the overall effort. The main objective of this article is to share the effective and robust test protocol that has been developed for small scale CO₂-SCC testing and the advances in the understanding of this phenomenon to-date. This combined electrochemical and applied load testing approach has shown that:

- The applied test protocol is key to achieve consistent and reproducible results. This includes an effective sample and solution preparation, a rigorous control of the applied final load and a well-controlled confined environment.
- CO₂ fugacity and applied stress are the main defining parameters however temperature and confinement also play an important role.
- The CO₂-SCC risk increases with CO₂ fugacity and confinement. The optimal temperature for reproducing CO₂-SCC was identified to be 40°C.
- At 100% of the AYS, all carbon steel grades may suffer from CO₂-SCC at/ above 15 bar fCO₂ thus contradicting existing research published on the subject.

5 ACKNOWLEDGMENTS

The authors would like to thank all the people who have contributed to this work both inside and outside of TechnipFMC. In addition to IFPEN, the external partner laboratories The French Corrosion Institute (a RISE subsidiary), France and Sourtec Engenharia de Corrosao, Brazil have contributed significantly through the execution of the applied load tests. Their vast knowledge and experience is greatly appreciated. An immense thank you goes out to the engineers and technicians that have worked meticulously to provide the detailed results presented in this article.

6 REFERENCES

1. J. Kittel, F. Grosjean, L. Ke, C. Taravel-Condât, and N. Desamais, "Corrosive environment in the annulus of flexible pipes: pH measurements in confined conditions and under high pressure," in Proceedings Eurocorr, 2013, pp. 1–9.
2. S. Last, S. Groves, J. Rigaud, C. Taravel-Condât, J. Wedel-Heinen, R. Clements and S. Buchner, "Comparison of Models to Predict the Annulus Conditions of Flexible Pipe," in Proceedings of the Annual Offshore Technology Conference, 2002, pp. 619–628.

- 1 3. A. Rubin, S. Overby, T. S. Nielsen, M. H. Haarh, and J. Gudme, "Corrosion Rates Of Carbon Steel In Confined Environments." In
2 Proceedings NACE, 2012.
- 3 4. M. E. Mitzithra, J. Rothwell, S. Paul, and F. P. dos Santos, "Exploring High Pressure CO₂ Annular Corrosion in Flexible Pipes." In
4 Proceedings NACE, 2020.
- 5 5. E. Remita, B. Tribollet, E. Sutter, F. Ropital, X. Longaygue, J. Kittel, C. Taravel-Condât and N. Desamais, "A Kinetic Model for CO₂
6 Corrosion of Steel in Confined Aqueous Environments," in Journal of The Electrochemical Society, 2008, vol. 155, no. 1, p. C41, doi:
7 10.1149/1.2801349.
- 8 6. F. Ropital, C. Taravel-Condât, J. N. Saas, and C. Duret, "Methodology to study the general corrosion of steel armours in simulated
9 conditions of flexible pipe annulus influence of confinement and evaluation of the pH," In The European Corrosion Congress, 2000.
- 10 7. E. Remita. F. Ropital, J. Kittel, B. Tribollet, "Experimental and theoretical investigation of the uniform corrosion in the annulus of
11 offshore flexible pipelines." In Proceedings NACE, 2008.
- 12 8. R. A. De Motte, "A Combined Experimental and Modelling Approach to Elucidate FeCO₃ Scale Formation Kinetics," Ph.D. thesis diss,
13 University of Leeds, 2016.
- 14 9. W. Li, B. Brown, D. Young, and S. Nešić, "Investigation of Pseudo-Passivation of Mild Steel in CO₂ Corrosion," Corrosion, vol. 70, no.
15 3, pp. 294–302, 2014.
- 16 10. G. R. Joshi et al., "Temporal evolution of sweet oilfield corrosion scale: Phases, morphologies, habits, and protection," Corros. Sci.,
17 vol. 142, pp. 110–118, 2018.
- 18 11. M. Gao, X. Pang, and K. Gao, "The growth mechanism of CO₂ corrosion product films," Corros. Sci., vol. 53, no. 2, pp. 557–568, Feb.
19 2011.
- 20 12. R. De Motte et al., "A study by electrochemical impedance spectroscopy and surface analysis of corrosion product layers formed
21 during CO₂ corrosion of low alloy steel," Corros. Sci., vol. 172, no. February, p. 108666, 2020.
- 22 13. T. Tanupabrungsun, B. Brown, and S. Nestic, "Effect of pH on CO₂ Corrosion of Mild Steel at Elevated Temperatures." In Proceedings
23 NACE, 2013.
- 24 14. B. Kinsella, Y. J. Tan, and S. Bailey, "Electrochemical Impedance Spectroscopy and Surface Characterization Techniques to Study
25 Carbon Dioxide Corrosion Product Scales," Corrosion, vol. 54, no. 10, pp. 835–842, 1998.
- 26 15. M. E. Orazem and B. Tribollet, "Electrochemical Impedance Spectroscopy," Electrochem. Impedance Spectrosc., pp. 1–523, Feb.
27 2008, doi: 10.1002/9780470381588.
- 28 16. A. Khalifeh, "Stress Corrosion Cracking Damages," Fail. Anal., Sep. 2019, doi: 10.5772/INTECHOPEN.80826.
- 29 17. "Alerta de Segurança 001-ANP/SSM: Corrosão sob Tensão por CO₂ (SCC-CO₂)." [https://www.gov.br/anp/pt-
30 br/assuntos/exploracao-e-producao-de-oleo-e-gas/seguranca-operacional-e-meio-ambiente/incidentes/arquivos/alertas-de-
31 seguranca/alerta-01/alerta-de-seguranca_001_ssm_scc-co2_pt.pdf](https://www.gov.br/anp/pt-br/assuntos/exploracao-e-producao-de-oleo-e-gas/seguranca-operacional-e-meio-ambiente/incidentes/arquivos/alertas-de-seguranca/alerta-01/alerta-de-seguranca_001_ssm_scc-co2_pt.pdf) (accessed Oct. 14, 2021).
- 32 18. W. Chen, "An Overview of Near-Neutral pH Stress Corrosion Cracking in Pipelines and Mitigation Strategies for Its Initiation and
33 Growth," Corrosion, vol. 72, no. 7, pp. 962–977, Jul. 2016.
- 34 19. M. A. Mohtadi-Bonab, "Effects of different parameters on initiation and propagation of stress corrosion cracks in pipeline steels: A
35 review," Metals (Basel), vol. 9, no. 5, May 2019.
- 36 20. G. Van Boven, W. Chen, and R. Rogge, "The role of residual stress in neutral pH stress corrosion cracking of pipeline steels. Part I:
37 Pitting and cracking occurrence," Acta Mater., vol. 55, no. 1, pp. 29–42, 2007.
- 38 21. J. Q. Wang and A. Atrens, "SCC initiation for X65 pipeline steel in the 'high' pH carbonate/bicarbonate solution," Corros. Sci., vol. 45,
39 no. 10, pp. 2199–2217, 2003.
- 40 22. T. Campos, J. A. Gomes, M. Seiersten, S. Palenscar, A. Dugstad, "Corrosion of Armor Wire Steel in the Annulus of Flexible Pipes at
41 Near Neutral pH." In Proceedings NACE, 2019.
- 42 23. J.A. Colwell, B. N. Leis, P.M Singh, "The Mechanism Of Near Neutral Ph SCC," In Proceedings NACE, 2005.
- 43 24. S. Asher, P. M. Singh, J. A. Colwell, B. N. Leis, "Stress Corrosion Cracking of Pipeline Steel in Near-Neutral pH Environments," In
44 Proceedings NACE, 2006.

25. R. N. Parkins and S. Zhou, "The stress corrosion cracking of C-Mn steel in CO₂-HCO₃-CO₂-3 solutions. I: Stress corrosion data," *Corros. Sci.*, vol. 39, no. 1, pp. 159–173, 1997.
26. TM0316-2016, "Standard Test Method Four-Point Bend Testing of Materials for Oil and Gas Applications," NACE, 2016.
27. TM0177-2005, "Standard Test Method Laboratory Testing of Metals for Resistance to Sulfide Stress Cracking and Stress Corrosion Cracking in H₂S Environments," NACE, 2005.
28. "ASTM D1141 - 98(2021) Standard Practice for Preparation of Substitute Ocean Water." <https://www.astm.org/Standards/D1141> (accessed Oct. 14, 2021).
29. H. Katayama, K. Noda, M. Yamamoto, and T. Kodama, "Relationship between corrosion rate of carbon steel and water film thickness under thin layer of artificial sea water," *Nippon Kinzoku Gakkaishi/Journal Japan Inst. Met.*, vol. 65, no. 4, pp. 298–302, 2001.
30. T. das Chagas Almeida, M. C. E. Bandeira, R. M. Moreira, and O. R. Mattos, "New insights on the role of CO₂ in the mechanism of carbon steel corrosion," *Corros. Sci.*, vol. 120, pp. 239–250, 2017.
31. R. A. De Motte, R. Barker, D. Burkle, S. M. Vargas, and A. Neville, "The early stages of FeCO₃ scale formation kinetics in CO₂ corrosion," *Mater. Chem. Phys.*, vol. 216, no. April, pp. 102–111, 2018.
32. F. Santos, I. Poloponsky, S. Modiano, C. Ribeiro, and E. Motta, "Evaluation of the SCC-CO₂ susceptibility of flexible pipe tensile armor wires," 2020.
33. W. Sun and S. Nešić, "Kinetics of Corrosion Layer Formation. Part 1-Iron Carbonate Layers in Carbon Dioxide Corrosion," *Corrosion*, vol. 64, no. 4, pp. 334–346, 2008.

7 FIGURE CAPTIONS

FIGURE 1. Layers of a typical flexible pipe

FIGURE 2. SEM images of typical CO₂-SCC cracks observed on flexible pipe armour wires retrieved from service operating in medium to high CO₂ environments (> 50 bar fCO₂ in the bore).

FIGURE 3. Photo of open autoclave prior to testing for (a) a 4pB Test configuration (b) tensile load test configuration

FIGURE 4. SEM Images of the cross-sectional microstructure of the different material steels studied (a) Steel A (b) Steel B (c) Steel C. Microstructure was obtained after etching in a 10% nital solution.

FIGURE 5. Schematic showing (a) 4pB Test configuration (b) Tensile Test configuration.

FIGURE 6. Microscope images identifying SCC crack profiles observed on Steel A tested under tensile load at 100% of the AYS and at conditions 40°C, 6 bar fCO₂.

FIGURE 7. SEM/ EDX analysis of observed corrosion deposit within the crack path. Test conditions: Steel A tested under tensile load at 100% of the AYS and at conditions 40°C, 6 bar fCO₂.

FIGURE 8. Microscope and SEM analysis of observed corrosion deposits in both the immersed and non-immersed region of the test sample. Test conditions: Steel C tested under tensile load at 100% of the AYS and at conditions 40°C, 12 bar fCO₂.

FIGURE 9. Cross-sectional SEM analysis of corrosion deposits in (a) immersed and (b) non-immersed region of the test sample. Test conditions: Steel C tested under tensile load at 100% of the AYS and at conditions 40°C, 12 bar fCO₂.

FIGURE 10. Photo of non-immersed region of the test sample (a) before and (b) after scale removal. Test conditions: Steel C tested under tensile load at 100% of the AYS and at conditions 40°C, 12 bar fCO₂.

FIGURE 11. 4pB test results studying the impact of temperature on Steel B at varying levels of stress and at 10.1 bar fCO₂. Top view microscopic and cross sectional SEM images show intensity and profile of CO₂-SCC cracks observed at 40 and 80°C, 100% AYS.

FIGURE 12. Nyquist plots showing comparison of impedance test results over time for Steel B at (a-b) 25°C, (c-d) 40°C, (e-f) 80°C and 10.1 bar fCO₂ at different time periods.

FIGURE 13. Mass loss corrosion rate results for Steel B exposed to 10.1 bar fCO₂ over test duration of 8 weeks at 25, 40 and 80 °C. Figure indicates SEM images showing the film characteristics for sample coupons examined at the end of test at the conditions tested.

FIGURE 14. Instantaneous corrosion rate over time determined from impedance measurements for Steel B tested at 10.1 bar fCO_2 and at 25, 40 and 80°C.

FIGURE 15. Microscope and SEM images identifying crack indications and SCC crack profiles observed on Steel B tested under tensile load at 95% of the AYS and at conditions 40°C, 6 bar fCO_2 .

FIGURE 16. Microscope, MPI and SEM image analysis identifying crack indications and SCC crack profiles observed on Steel C tested under tensile load at 100% of the AYS and at conditions 40°C, 15 bar fCO_2 .

FIGURE 17. Nyquist plots showing impedance test results over time for Steel C at 40°C, 10.1 bar fCO_2 and (a-b) $V/S = 1$, (c-d) $V/S = 0.3$ over different time periods.

FIGURE 18. SEM image analysis identifying crack indications and SCC crack profiles observed on Steel A tested under tensile load at 100% of the AYS over a duration of 6 months and at conditions 40°C, (a) 3 bar fCO_2 (b) 6 bar fCO_2 .

FIGURE 19. Nyquist plot showing impedance test results over time for Steel C at $V/S = 1$, 40°C and (a) 1 bar fCO_2 , (b) 15 bar fCO_2 , (c) 22 bar fCO_2

8 TABLES

Table 1. Description of materials tested including the carbon chemical composition in weight %.

Material	Application	Microstructure	Yield Strength 0.2% (MPa)	Ultimate Tensile Strength (MPa)	C (weight %)
Steel A	Sweet Service	Ferrite-pearlite	> 1100	1400 - 1600	0.6 - 0.75
Steel B	Slightly sour service	Ferrite-pearlite	≥ 1080	1200 - 1280	0.6 - 0.75
Steel C	Sour Service	Tempered martensite	> 700	780 - 860	0.3 – 0.38

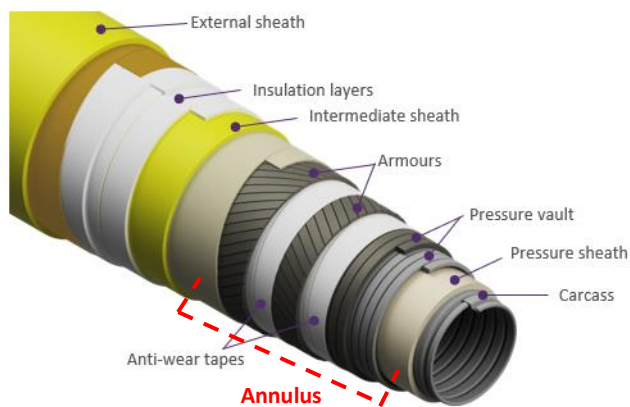


Figure 1.

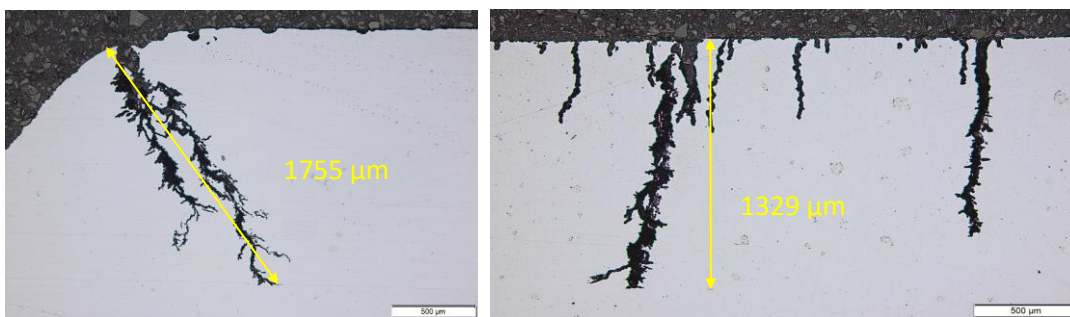


Figure 2.

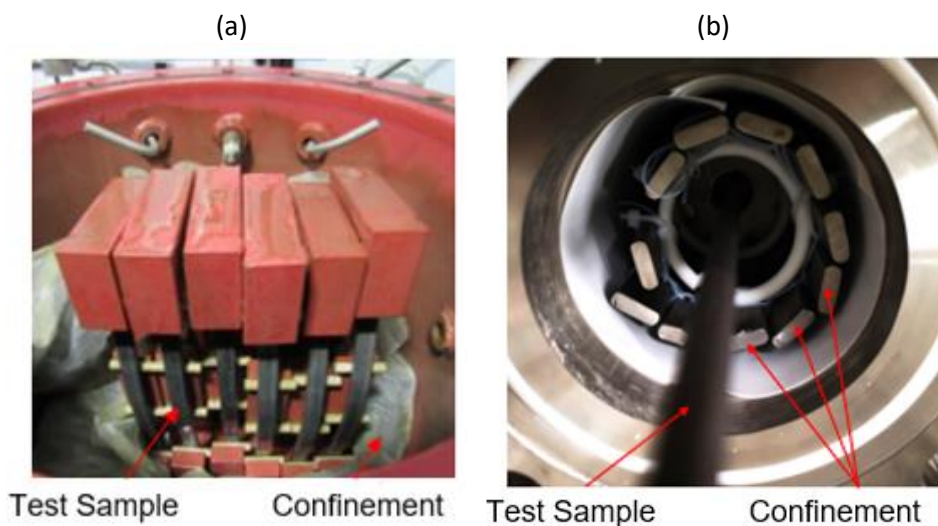


Figure 3.

1
2
3
4
5
6
7
8
9
10
11
12
13
14
15
16
17
18
19
20
21
22
23
24
25
26
27
28
29
30
31
32
33
34
35
36
37
38
39
40
41
42
43
44
45
46
47
48
49
50
51
52
53
54
55
56
57
58
59
60



Figure 4.

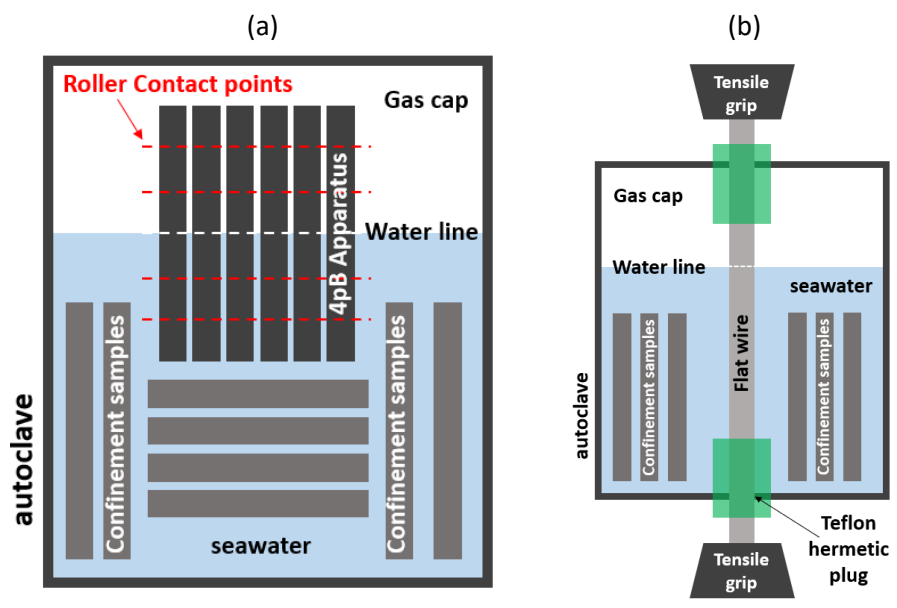


Figure 5.

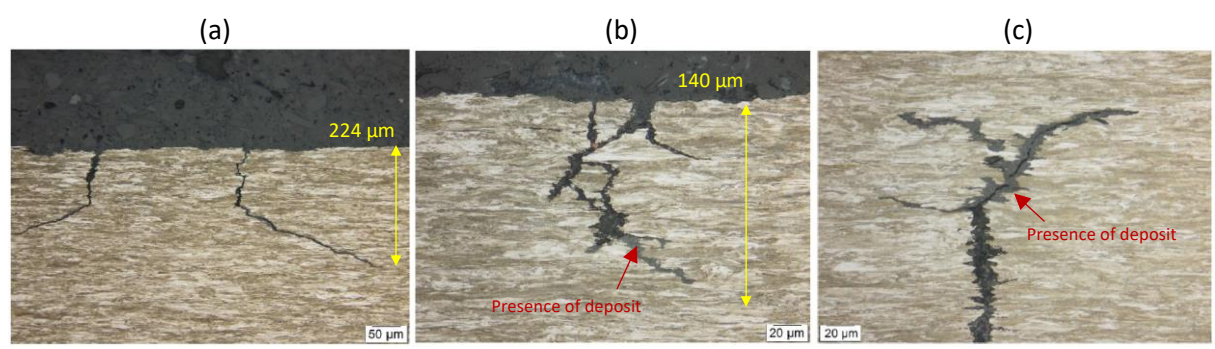


Figure 6.

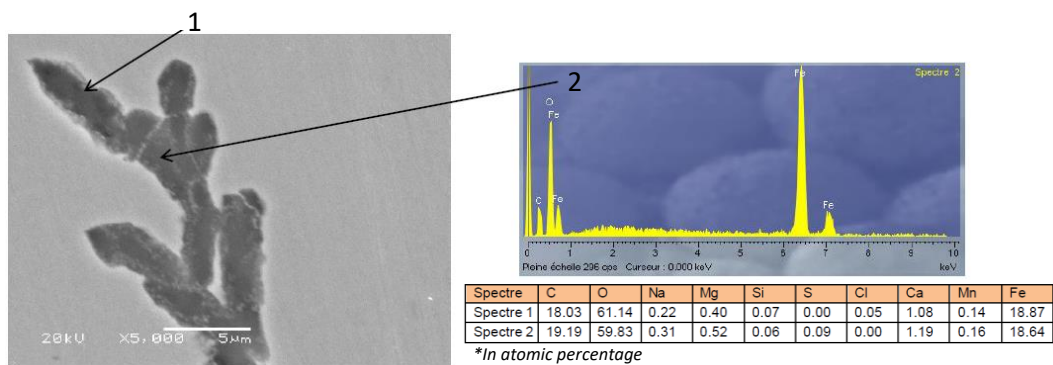


Figure 7.

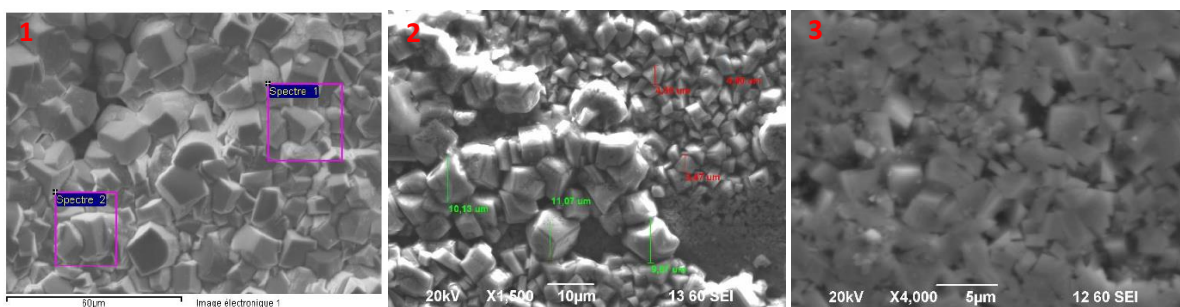
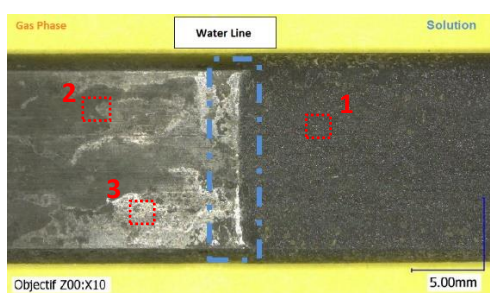


Figure 8.

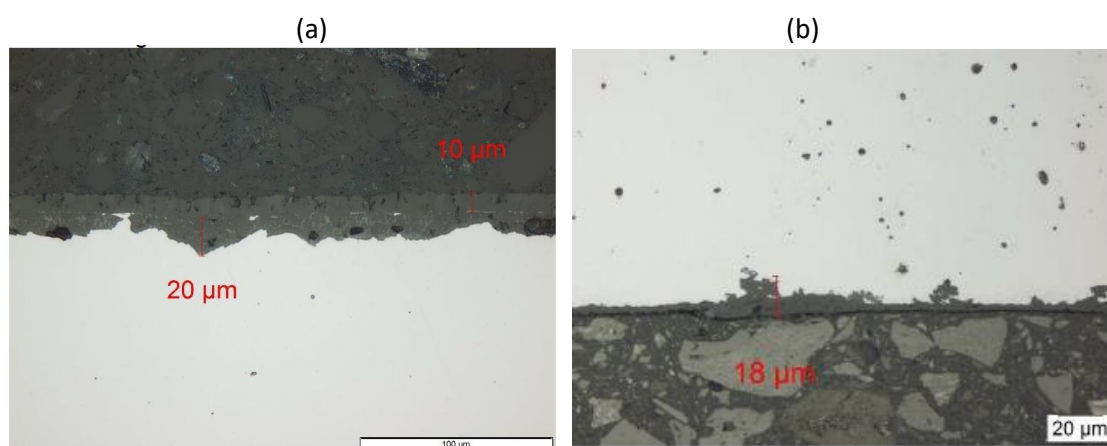


Figure 9.

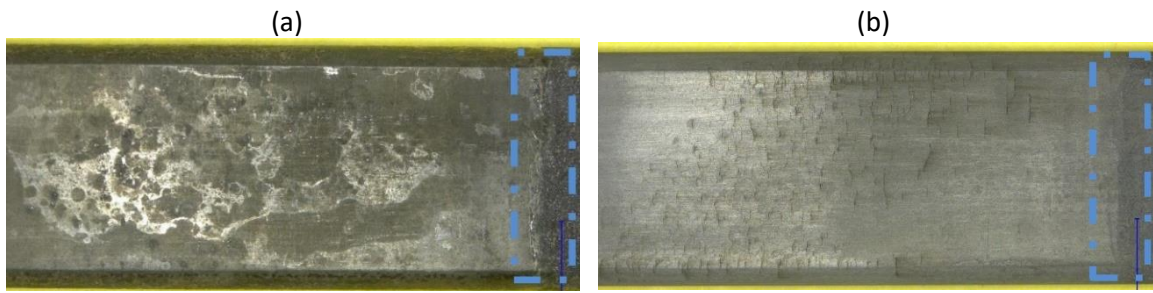


Figure 10.

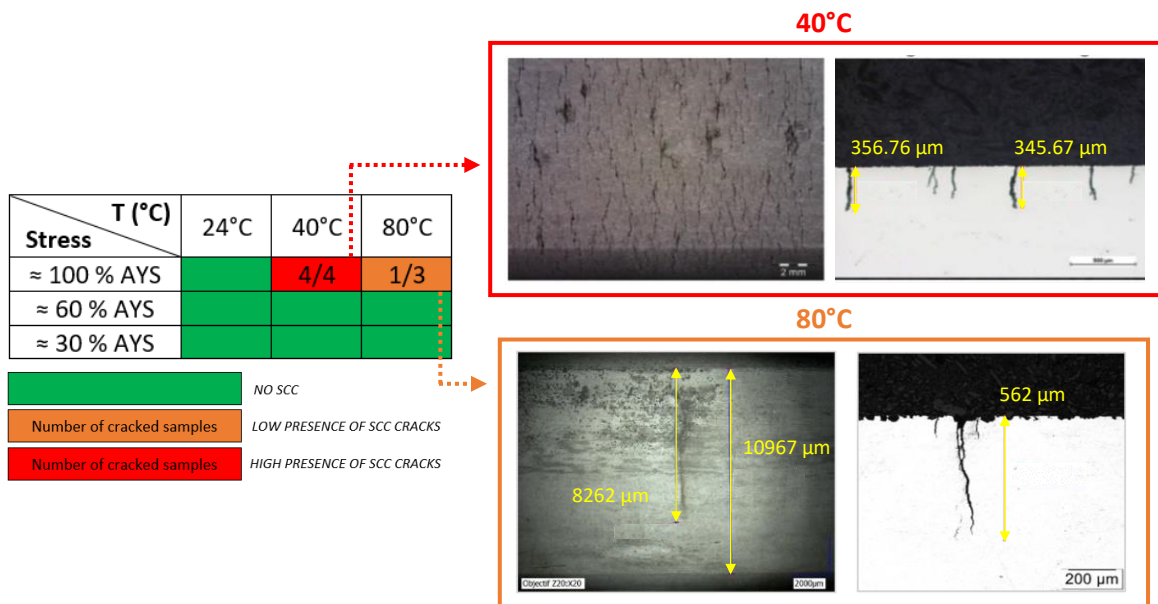


Figure 11.

1
2
3
4
5
6
7
8
9
10
11
12
13
14
15
16
17
18
19
20
21
22
23
24
25
26
27
28
29
30
31
32
33
34
35
36
37
38
39
40
41
42
43
44
45
46
47
48
49
50
51
52
53
54
55
56
57
58
59
60

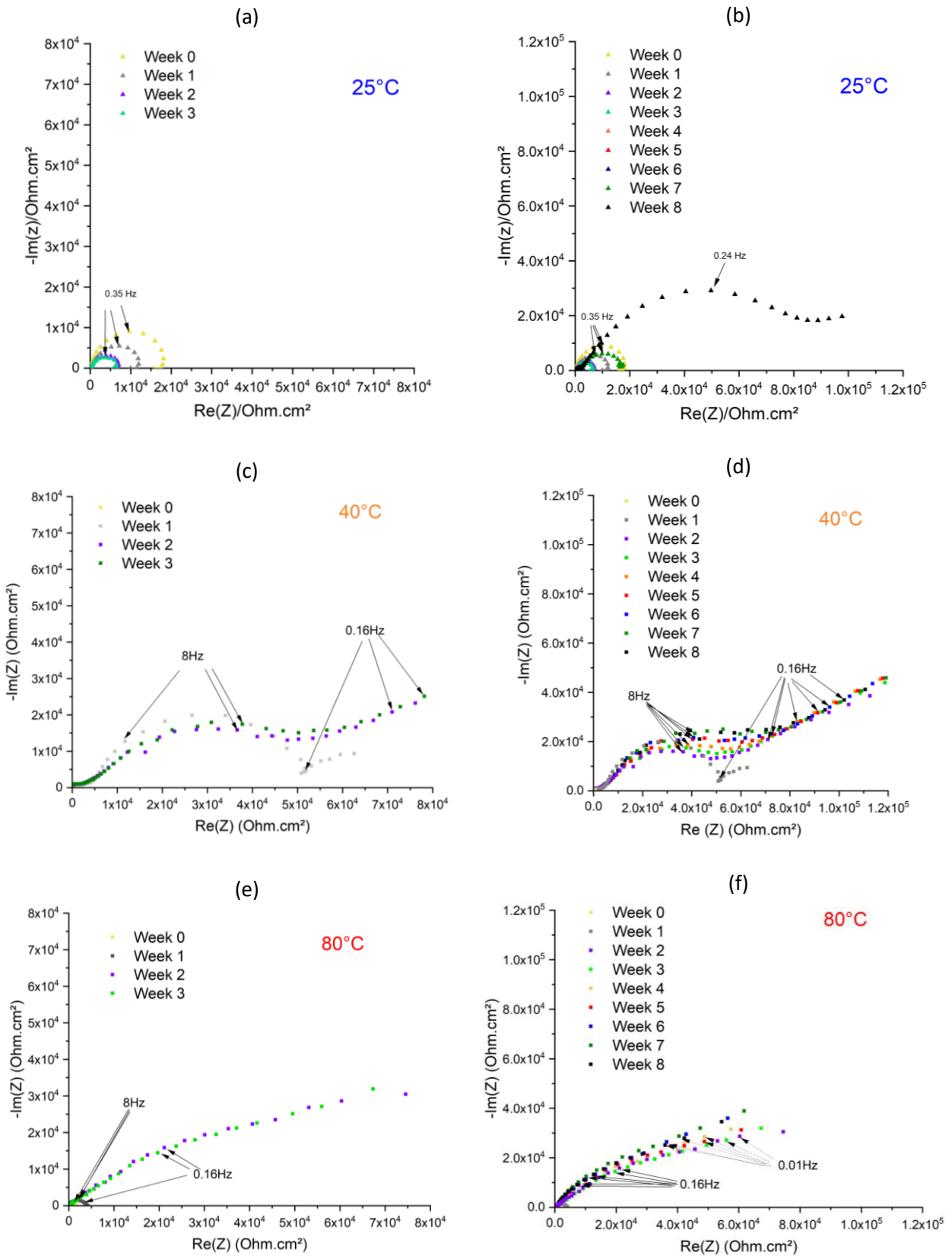


Figure 12.

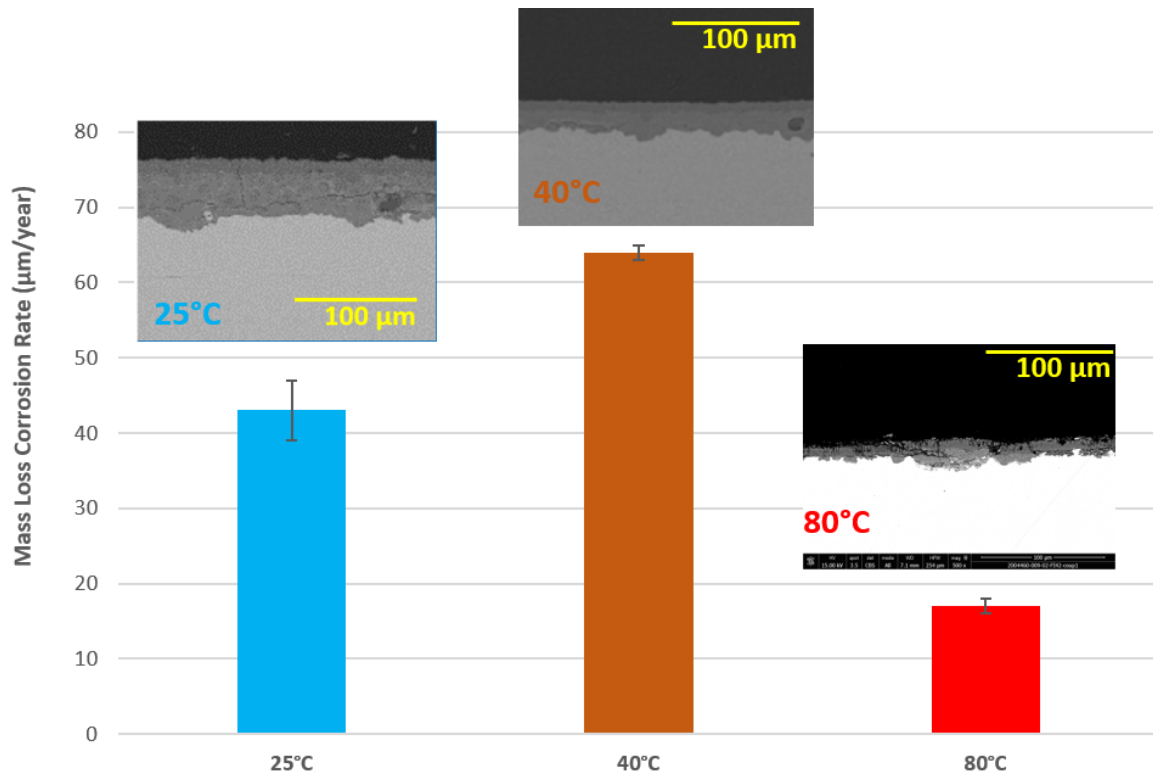


Figure 13.

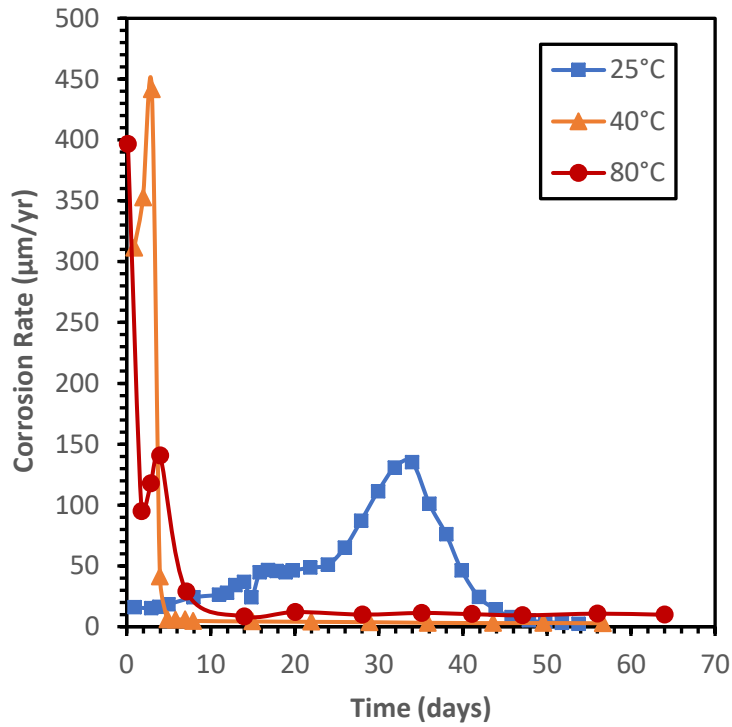


Figure 14.

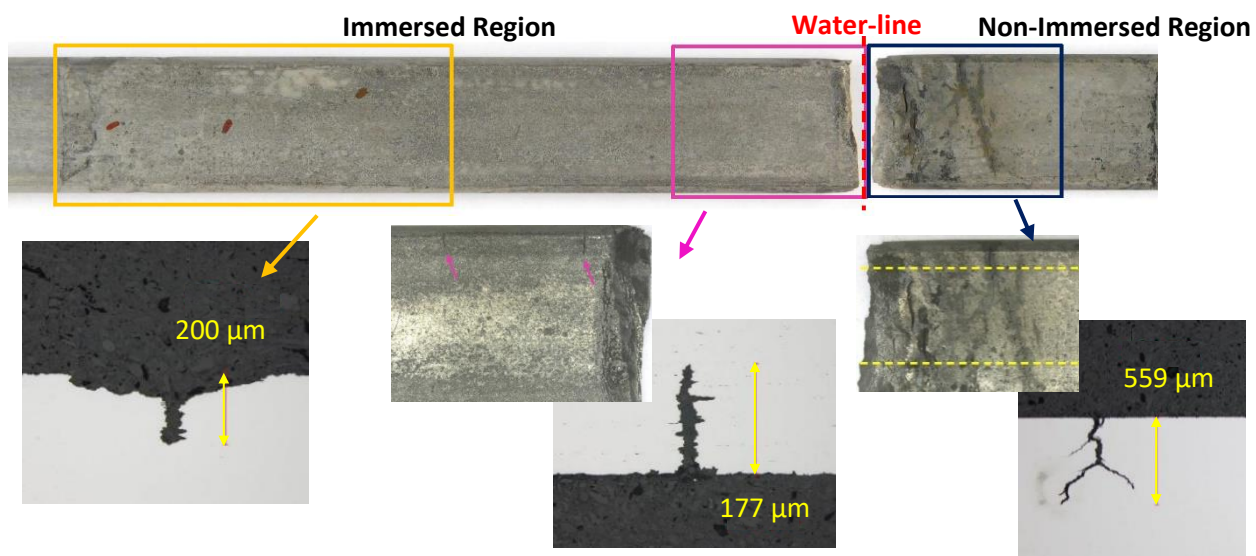


Figure 15.

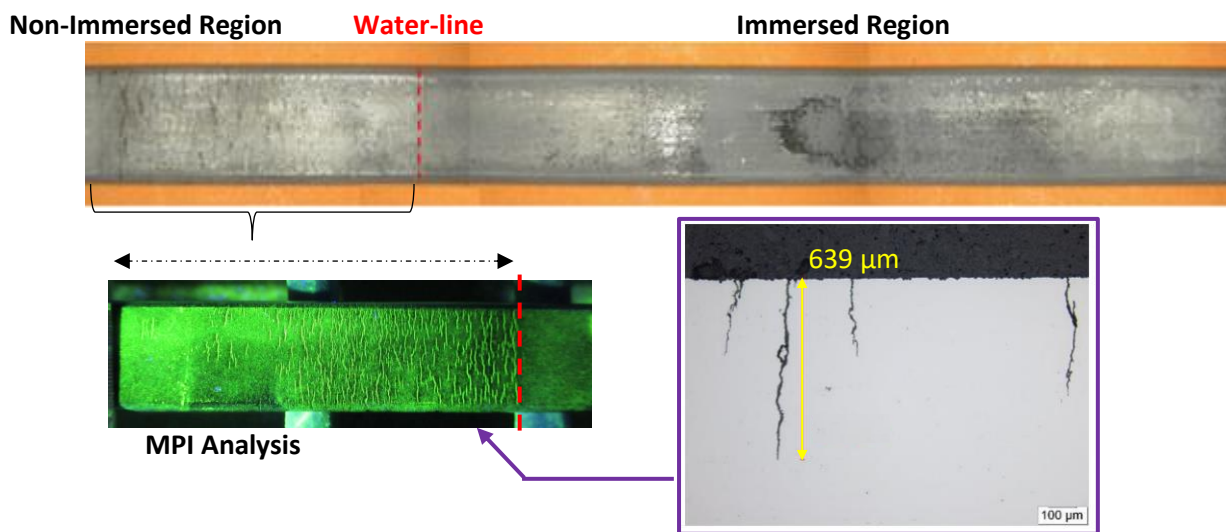


Figure 16.

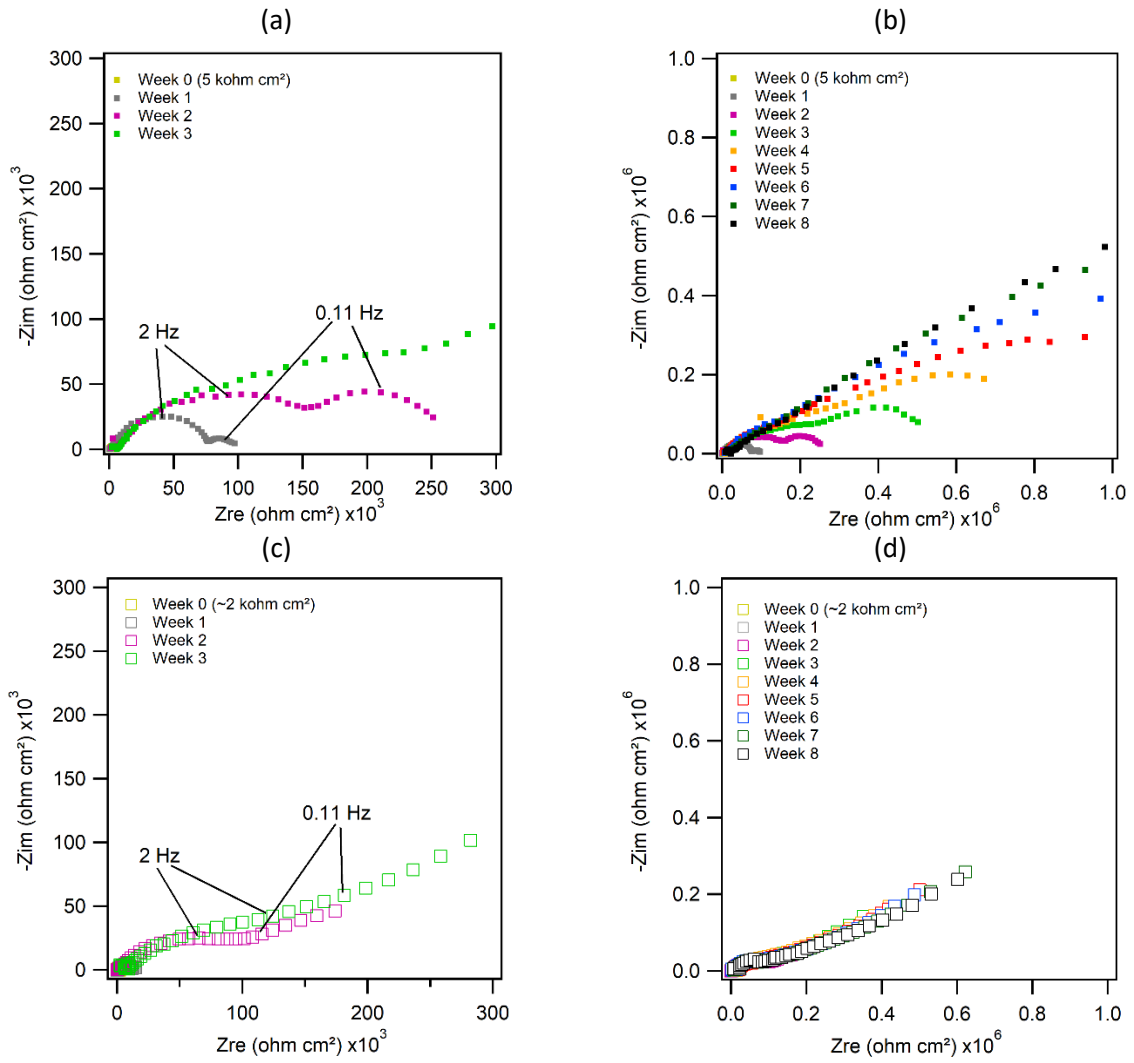


Figure 17.

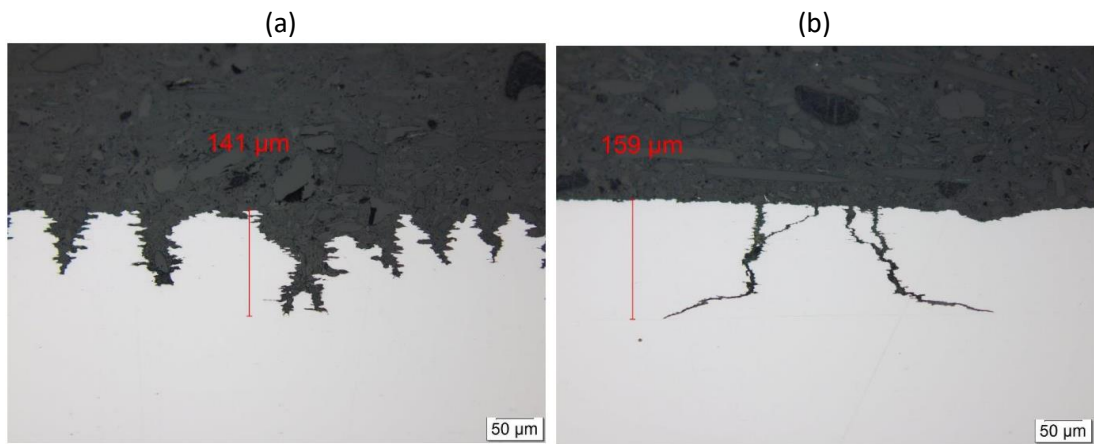


Figure 18.

